Petrology and geochemistry of spinel peridotite nodules and host basalt, Vestspitsbergen

H. FURNES, R. B. PEDERSEN & S. MAALØE

Furnes, H., Pedersen, R. B. & Maaløe, S.: Petrology and geochemistry of spinel peridotite nodules and host basalt, Vestspitsbergen. *Norsk Geologisk Tidsskrift,* Vol. 66, pp. 53–68. Olso 1986. ISSN 0029-196X.

Mineral compositions and major and trace element whole-rock analyses for eight spinel peridotite nodules and their host basalt from Quaternary volcanoes in Vestspitsbergen are presented. Modally the nodules range from harzburgite, lherzolite (dominant) and olivine websterite, and they are considered to represent mantle material. The olivines range in composition from Fo 88.1 to 92.0, the orthopyroxenes have 100 Mg /(Mg + Fe^t) ratios between 88.9 to 92.3. The clinopyroxenes are chrome-diopside and the oxide phase is Al- or Cr-spinel.

The compatible trace elements of the nodules correlate with their modal composition. Thus Sc correlate positively with clinopyroxene, whereas Ni and Co correlate positively with olivine. La, Ta, Th, U and K show highest concentrations in some of the most refractory nodules, and their REE patterns are very variable.

The refractory nature of some of the nodules is thought to relate to an earlier basalt extraction from the mantle. This 'refractory' mantle was subsequently enriched in the highly incompatible elements, probably by the veining or the metasomatism by alkali basalt. The host basalt can be modelled, in terms of RE elements, to represent a partial melt (around 3% batch melting) of a composite source, represented by the spinel peridotites nodules.

H. Furnes, R. B. Pedersen & S. Maaløe, Geologisk Institutt, avd. A, Allé gt. 41, 5014 Bergen, Norway.

Ultramafic nodules brought to the surface by volcanic eruptions, usually by alkaline volcanites, may either represent accidental material sampled by the ascending magma, or cognate cumulates. In the former case important information about the history of the source area for basaltic rocks is provided (e.g. Frey & Prinz 1978, Delaney et al. 1979, Maaløe & Printzlau 1979, Kurat et al. 1980, Ehrenberg 1982, Kyser et al. 1982, Griffin et al. 1984).

The Quaternary volcanoes Sverrefjellet, Halvdanpiggen and Sigurdfjellet on the eastern side of Woodfjorden in Vestspitsbergen (Fig. 1) contain abundant ultramafic xenoliths (Hoel 1914, Gjelsvik 1963), ranging in composition from spinel peridotites, spinel and garnet pyroxenites, pyroxene granulites and other rocks of shallow crustal origin (Foss Amundsen 1984).

The present account deals with petrography, mineral and bulk chemistry of eight samples of spinel peridotites (seven from Sverrefjellet and one from Sigurdfjellet) collected by Dr. T. Gjelsvik. A model for their evolution (based on mineral chemistry, major and trace elements of the bulk rock), as well as the petrogenesis of the host basalt (based on the REE data for the basalt and spinel peridotites), are presented. T and P es-

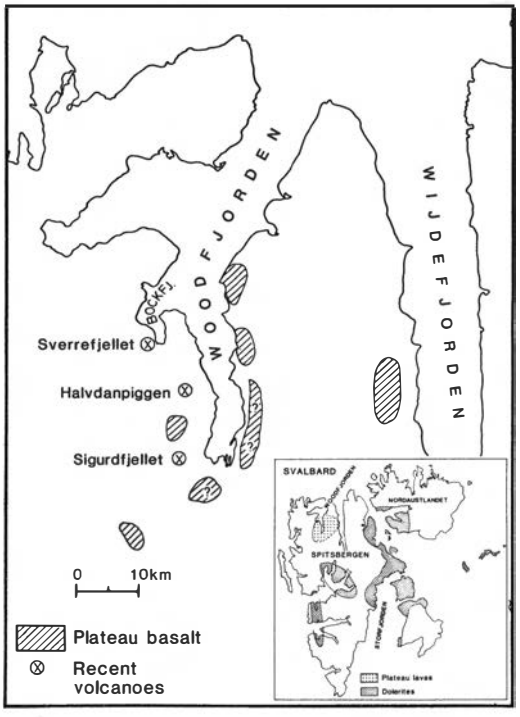

Fig. 1. Location map of the Sverrefjellet, Haldanpiggen and Sigurdfjellet volcanoes (Modified from Prestvik (1978)).

timates have not been attempted, but for general information the reader is referred to the P/T diagram of Carswell (1980).

Analytical methods

The electron microprobe analyses were carried out by standard wavelength dispersive methods (Reed 1975), using an accelerating voltage of 15 KV and a beam current of 10 nA. A mixture of minerals, synthetic oxides and pure metals were employed as standards. Net peak intensities, corrected for dead-time effects and beam-current drift, were reduced by MAGIC IV (Colby 1968).

The major-oxide composition (except Na_2O and K_2O which were analysed by atomic absorption) and the trace elements V, Cr, Ni and Zn were determined by X-ray fluoresence spectroscopy. International standards and Flanagan's (1973, 1976) recommended values were used for calibration. The major oxides were analysed using glass beads prepared by the method of Padfield & Gray (1971). The trace elements were determined in powder briquettes and adjusted for major-oxide mass absorption effects. The RE elements and Cs, Hf, Ta, Th, U, Sc and Co were determined by both instrumental and radiochemical neutron activation, using international standards. Methods are described by Brunfelt & Steinnes (1969, 1971), Covell (1959), Sterlinski (1968), Anders (1969) and Baedecker et al. (1977).

Petrography and geochemistry of the host basalt of Sverrefjellet

The host basalt contains microphenocrysts predominantly of olivine (Fo 83.4), with smaller amounts of clinopyroxene ($En_{37.2}$ $Fs_{13.4}$ $Wo_{49.4}$) and tiny laths of plagioclase ($An_{55.4}$ $Ab_{42.1}$ $Or_{2.5}$), set in a dark, dense to tachylitic groundmass.

The bulk rock analysis represents a large number of small, handpicked fragments, visually free of xenoliths, sampled from one piece of rock. The major and trace element composition is shown in Table 1. The concentrations of Na_2O, K_2O and the incompatible trace elements Cs, Hf, Ta, Th, U and LREE are high, and would classify the host as an alkali basalt or basanite. Its REE pattern (Fig. 2) shows strong enrichment from Tb through La, but a flat pattern from Tb through Lu, the latter with concentrations approximately 30 times chondrite. The MREE to LREE thus define the pattern characteristic of alkaline basaltic rocks, whereas the HREE is more akin to tholeiitic basalts.

Table 1. Major and trace element analyses of the host basalt

SiO_2	46.12	La	36.77	Sc	15.38
TiO_2	2.62	Ce	84.97	V	224
Al_2O_3	14.34	Sm	8.62	Cr	229
Fe_2O_3	3.39	Eu	2.55	Co	42
FeO	6.97	Gd	8.28	Ni	187
MgO	9.23	Tb	0.93	Zn	96
CaO	8.69	Ho	1.40		
Na_2O	5.12	Tm	0.61		
K_2O	1.78	Yb	4.63		
MnO	0.16	Lu	0.68		
P_2O_5	0.73				
L.o.i.	0.87	Cs	1.11		
		Hf	6.24		
Total	100.02	Ta	3.65		
Mg/Mg		Th	4.90		
+Fe	0.621	U	1.98		

The nodules

The nodule from Sigurdfjellet (Fig. 1) (sample 5) occurs in a pyroclastic deposit. The Sverrefjellet samples are all (Fig. 1) hosted in basalt lavas. Sizes from a few mm up to around 10 cm are represented in the material examined for this account. The colour is yellowish-green. For more details of the Sverrefjellet volcano and its nodule-bearing basalt, the reader is referred to Gjelsvik (1963).

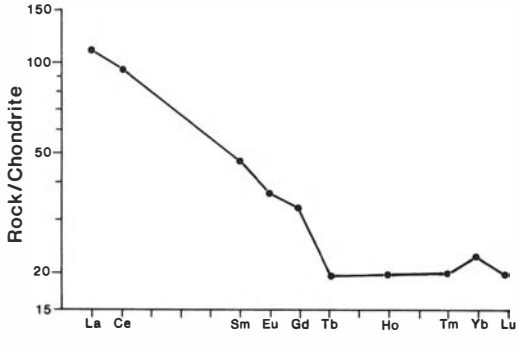

Fig. 2. Chrondrite-normalized REE pattern of the host basalt. Chondrite data from Haskin et al. (1968).

Table 2. Modes based on point counting (PC) and mass balance (MB) of the spinel peridotites

Reference nos.	1		2		3		4		5		6		7			8	
Sample nos.	GJ63.98		GJ63.97		GJ63.95		GJ62.23		GJ75.159I		GJ62.14		GJ62.21			GJ63.96	
Method	PC	MB	PC	MB	PC	MB	PC	MB	PC	MB	PC	MB	PC1	PC2	MB	PC	MB
Olivine	76.7	69.7	89.0	72.7	88.3	78.9	62.4	63.2	79.7	78.5	–	57.9	63.0	79.9	54.5	–	27.1
Orthopyroxene	16.0	23.1	5.1	20.6	10.6	17.9	36.4	33.5	11.5	11.4	–	24.6	22.3	16.5	34.0	–	48.4
Clinopyroxene	4.8	5.9	4.9	5.3	0.1	1.9	0.6	2.3	6.0	8.1	–	15.1	11.8	2.6	9.4	–	21.0
Spinel	2.5	1.3	0.9	1.4	1.0	1.4	0.6	1.0	2.8	1.9	–	2.4	3.0	0.9	2.1	–	3.5
Amphibole									tr								
Glass					tr						tr						

tr = trace

Modal proportions

The modal proportions have been determined by point counting both thin sections and major element mass balance, the latter by using bulk rock and mineral compositions of each sample shown in Tables 3–7 and Table 11. The results are shown in Table 2, and compositionally the nodules range from harzburgites and lherzolites to olivine websterite. The results of point counting and mass balance estimation may show pronounced different results (samples 2, 3 and 7), to nearly identical results (samples 4 and 5). The marked discrepancies are most probably due to modal variations within samples,as indicated by the point counting results of two thin sections from sample 7, showing entirely different results (Table 2). It is thus believed that the mass balance calculations give more correct results since each nodule becomes homogenized during crushing. The oxide residues for each mass balance calculation are good, except for iron, which in most cases gives too high values in the bulk rock (ca. 0.5 to 1 wt%). This could be compensated for by small amounts of iron oxide along some grain boundaries and spinel exolution in pyroxene which has not been accounted for.

Penetration of the host basalt into the nodules by following grain boundaries has been observed in some cases. To avoid the effect of such contamination in the bulk rock analyses as much as possible, each nodule was cut into thin slices, rejecting those in which one visually could trace basalt veins. In sample 6 there are minor concentrations of glass ($\ll$0.1%) (Table 8), which is considered as insignificant in disturbing the mass balance calculations.

Petrography

Texturally most of the nodules can be classified as protogranular (Mercier & Nicolas 1975), with the grain size of olivine and orthopyroxene ranging from 0.5 mm to 5 mm, and showing curvilinear grain boundaries. However, minor portions show polygonization and recrystallization of olivine and orthopyroxene into aggregates. These crystals are much smaller than those mentioned above. Two of the samples (6 and 8) show kinked orthopyroxene, and texturally these two may be classified as grading into weakly porphyroclastic. This is also shown by some parallel orientation of spinel (in sample 6). Sample 3 has an equidimensional grain size of around 2 mm. Grain boundaries may be curvilinear, but a high proportion are straight, and converge at 120° in triple points. This sample may be classified texturally as the equigranular type (Mercier & Nicolas 1975).

The clinopyroxene grains, mostly with a green tint, are generally smaller than the olivine and orthopyroxene grains, and in one observed case (in sample 7) clinopyroxene may occur as blebs in orthopyroxene. In a few cases exolution lamellae of clinopyroxene are observed in the central part of orthopyroxene host. Spinel grains, varying in colour from deep red to nearly black, are of highly variable size, from <0.5 mm up to 5 mm, and have always a vermicular shape. In sample 3 spinel has also been found as exolution lamellae in clinopyroxene. Amphibole (pargasite), with a weak greenish-brown pleochroism occurs as a trace constituent in sample 5.

Sample 6 contains several small patches (<1 mm) of colourless glass containing euhedral crystallites of olivine and spinel. The glass is always in contact with olivine and spinel, and sometimes also with clinopyroxene. Where the glass is in

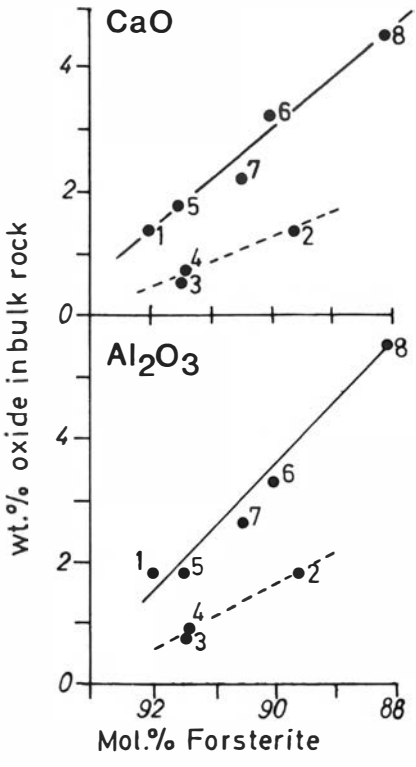

Fig. 3. Relationship between bulk rock CaO and Al_2O_3 and forsterite content of olivine in spinel peridotite nodules.

contact with spinel, the latter has a spongey appearance.

Mineral chemistry

Olivine. – The mole percent forsterite ranges between 88.1 and 92.0 (Table 3). Within-sample compositional variations are insignificant compared to those mentioned above. There is a systematic increase in the Fe-content as the bulk rock CaO and Al_2O_3 contents decrease (Fig. 3), a feature also demonstrated by Frey & Prinz (1978) in spinel peridotites. Two groups, one defined by samples 1, 5, 6, 7 and 8, and the other by samples 2, 3 and 4, seem to exist (Fig. 3). The latter is poorer in CaO and Al_2O_3 at a given Fo-content than the former.

Orthopyroxene. – The composition of orthopyroxenes are shown in Table 4. The 100 (Mg/Mg + Fe') ratios range from 88.9 in sample 8 to 92.3 in sample 1, and show a good positive correlation with the Fo-content of olivine, though the ortho-

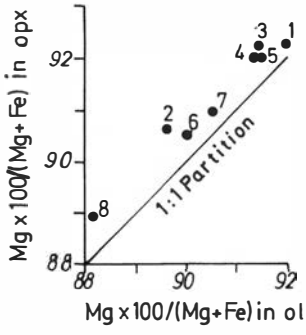

Fig. 4. The partitioning of Mg and Fe between olivine and orthopyroxene.

pyroxene values are slightly above the 1:1 partition line between the two minerals (Fig. 4). This feature was also demonstrated by Brown et al. (1980). Plotted in the Wo-En-Fs diagram, the orthopyroxene shows constant Wo-level. The oxides that show the most pronounced variations are Al_2O_3 and Cr_2O_3, ranging between 1.63–4.16 and 0.19–0.49 wt.%, respectively. A number of analyses across grains show no significant variations.

Clinopyroxene. – The composition of clinopyroxenes is shown in Table 5. In terms of Cr_2O_3 content (0.58–1.58 wt.%) and Wo: En: Fs relations,

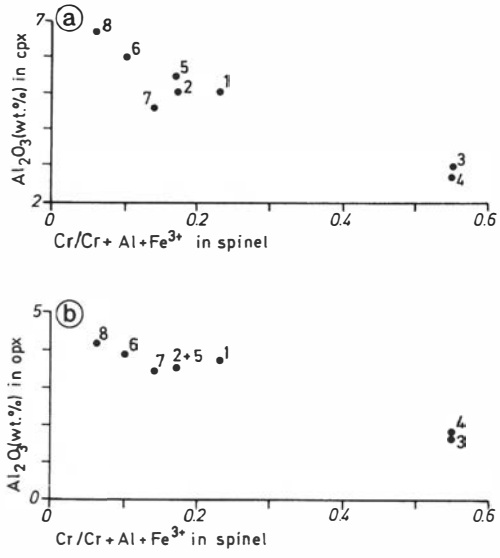

Fig. 5. Relationships between Cr/(Cr + Al + Fe^{3+}) vs. Al_2O_3 in clinopyroxene (a) and Al_2O_3 in orthopyroxene (b).

Table 3. Average microprobe analyses of olivine

Ref. nos.	1	2	3	4	5	6	7	8
Field nos.	GJ63.98	GJ63.97	GJ63.95	GJ62.23	GJ75.159I	GJ62.14	GJ62.21	GJ63.96
No. of anal.	3	4	3	4	14	5	3	3
SiO_2	40.18	40.43	40.80	41.06	40.11	40.21	40.44	40.55
FeO^t	7.82	9.99	8.31	8.47	8.09	9.75	9.06	11.44
MnO	0.09	0.20	0.13	0.14	0.14	0.14	0.14	0.15
NiO	0.30	0.35	0.36	0.36	0.35	0.37	0.37	0.32
MgO	50.70	49.22	50.43	50.56	48.78	49.47	48.22	47.71
CaO	0.07	0.04	0.06	0.03	0.04	0.05	0.03	0.04
Total	99.16	100.23	100.09	100.62	97.51	99.99	98.26	100.21
Cation formulae based on 24 oxygens								
Si	5.917	5.945	5.961	5.965	6.007	5.919	6.031	5.997
Fe	0.963	1.252	1.015	1.029	1.013	1.201	1.130	1.415
Mn	0.011	0.025	0.016	0.018	0.018	0.017	0.018	0.019
Ni	0.035	0.042	0.043	0.043	0.042	0.044	0.044	0.038
Mg	11.126	10.787	10.982	10.950	10.889	10.853	10.720	10.516
Ca	0.011	0.007	0.009	0.005	0.007	0.008	0.005	0.007
100 Mg/Mg+Fe^t	92.0	89.6	91.5	91.4	91.5	90.0	90.5	88.1

Table 4. Average microprobe analyses of orthopyroxene

Ref. nos.	1	2	3	4	5	6	7	8
Field nos.	GJ63.98	GJ63.97	GJ63.95	GJ62.23	GJ75.159I	GJ62.14	GJ62.21	GJ63.96
No. of anal.	4	4	3	3	13	5	3	3
SiO_2	55.09	55.06	54.84	56.77	54.18	54.63	54.68	54.78
TiO_2	0.11	0.02	0.06	0.02	0.04	0.09	0.07	0.13
Al_2O_3	3.71	3.49	1.63	1.75	3.50	3.90	3.40	4.16
Cr_2O_3	0.49	0.36	0.39	0.47	0.34	0.29	0.27	0.19
FeO^t	5.03	6.17	5.15	5.38	5.09	6.18	5.82	7.28
MnO	0.14	0.13	0.16	0.13	0.12	0.14	0.13	0.18
NiO	0.06	0.08	0.14	0.08	0.10	0.12	0.09	0.13
MgO	33.96	33.40	34.17	34.89	32.84	33.09	33.05	32.56
CaO	0.64	0.56	0.48	0.54	0.55	0.42	0.45	0.45
Na_2O	0.08	0.10	0.11	0.11	0.05	0.06	0.05	0.08
Total	99.31	99.37	97.13	100.14	96.81	98.92	98.01	99.94
Cation formulae based on 24 oxygens								
Si	7.632	7.658	7.782	7.804	7.692	7.630	7.688	7.609
Ti	0.012	0.002	0.007	0.002	0.004	0.009	0.008	0.014
Al	0.606	0.571	0.272	0.284	0.586	0.642	0.564	0.681
Cr	0.062	0.039	0.044	0.050	0.038	0.033	0.035	0.075
Fe	0.582	0.717	0.610	0.618	0.604	0.722	0.684	0.845
Mn	0.017	0.015	0.020	0.015	0.014	0.017	0.015	0.021
Ni	0.007	0.009	0.016	0.009	0.011	0.013	0.011	0.014
Mg	7.014	6.926	7.214	7.148	6.950	6.887	6.924	6.742
Ca	0.095	0.084	0.073	0.080	0.084	0.063	0.068	0.067
Na	0.022	0.027	0.031	0.028	0.015	0.017	0.013	0.022
Ca/Ca + Mg	0.013	0.012	0.010	0.011	0.012	0.009	0.010	0.010
Mg/Mg + Fe^t	0.923	0.906	0.922	0.920	0.920	0.905	0.910	0.889
Wo	1.2	1.1	0.9	1.0	1.1	0.8	0.9	0.9
Fs	7.6	9.3	7.7	7.9	7.9	9.4	8.9	11.0
En	91.2	89.6	91.4	91.1	91.0	89.9	90.2	88.1

Table 5. Average microprobe analyses of clinopyroxene

Ref. nos.	1	2	3	4	5	6	7	8
Field nos.	GJ63.98	GJ63.97	GJ63.95	GJ62.23	GJ75.159I	GJ62.14	GJ62.21	GJ63.96
No. of anal.	3	6	1	3	14	3	3	4
SiO_2	51.70	52.00	54.38	53.95	50.96	51.82	51.67	51.64
TiO_2	0.39	0.35	0.18	0.00	0.31	0.46	0.18	0.78
Al_2O_3	5.07	5.06	3.00	2.68	5.53	5.98	4.57	6.68
Cr_2O_3	1.11	0.81	1.58	1.02	0.86	0.65	0.73	0.52
FeO^t	2.15	2.42	2.20	2.21	2.18	2.51	2.18	2.69
MnO	0.10	0.12	0.09	0.04	0.08	0.08	0.10	0.09
MgO	15.76	16.03	16.57	17.07	15.29	14.72	15.85	14.90
CaO	20.26	21.02	20.99	21.06	19.42	20.76	20.74	20.10
Na_2O	1.33	1.24	1.45	1.31	1.47	1.50	1.24	1.67
Total	97.87	99.05	100.44	99.34	96.10	98.48	97.26	99.07
Cation formulae based on 24 oxygens								
Si	7.622	7.600	7.828	7.842	7.639	7.619	7.675	7.535
Ti	0.043	0.038	0.019	0.000	0.034	0.051	0.021	0.086
Al	0.880	0.872	0.508	0.462	0.977	1.037	0.800	1.149
Cr	0.130	0.094	0.180	0.118	0.101	0.076	0.86	0.050
Fe	0.265	0.296	0.265	0.268	0.273	0.309	0.270	0.328
Mn	0.012	0.015	0.011	0.006	0.010	0.010	0.013	0.011
Mg	3.464	3.491	3.554	3.698	3.416	3.227	3.509	3.239
Ca	3.202	3.291	3.237	3.280	3.118	3.271	3.301	3.143
Na	0.381	0.351	0.406	0.368	0.428	0.428	0.356	0.477
Ca/Ca + Mg	0.48	0.49	0.48	0.47	0.52	0.50	0.48	0.49
Mg/Mg + Fe^t	0.929	0.922	0.931	0.937	0.926	0.913	0.929	0.908
Wo	46.2	46.5	45.9	45.3	45.8	48.1	46.6	46.8
Fs	3.8	4.2	3.8	3.7	4.0	4.5	3.8	4.9
En	50.0	49.3	50.3	51.0	50.2	47.4	49.6	48.3

the clinopyroxene can be classified as chrome diopside. TiO_2 and Al_2O_3 vary considerably, from 0–0.78 and 2.68–6.68 wt.%, respectively. The highest content of Al_2O_3 in clinopyroxene is found in sample 8, which has also the highest Al_2O_3 in orthopyroxene (Table 4) and the lowest Fo of olivine (Table 3). No within-grain variations have been observed.

Spinel. – Spinel compositions are shown in Table 6. Large compositional variations exist with respect to FeO^t, Al_2O_3 and Cr_2O_3, particularly the latter oxide, that varies between 5.65–45.44 wt.%. As the Cr/(Cr. + Al + Fe^{3+}) in the spinel increases, the Al_2O_3 in coexisting clinopyroxene and orthopyroxene decreases (Fig. 5a,b). Carswell (1980) proposed that nodules of mantle origin should be divided into three classes on the basis of their spinel compositions: Al-spinel, Cr-spinel, and chromite lherzolites with spinel compositions 100 Cr/(Cr + Al) < 25, 25–65, and > 65, respectively. The spinels of the Spitsbergen nodules are Al-spinels except for those in samples 3 and 4 which are Cr-spinels (Table 6, Fig. 5a,b), and the rocks may accordingly be termed Al-spinel and Cr-spinel peridotites.

Amphibole. – Amphibole has only been found in the Sigurdfjellet sample (sample 5), and its composition is shown in Table 7. According to Leake (1978) it can be classified as pargasite.

Intra-nodule glass. – Intra-nodule glass, occurring as round, elongated or irregularly-formed blebs, ranging in size from < 0.1 mm to 0.5 mm in diameter, is abundant in sample 6. The colourless glass, in some cases vesicular (Fig. 6), is always in contact with spinel and olivine, and sometimes also with clinopyroxene. It contains variable amounts of euhedral olivine crystallites and in a few cases, spinel. The chemical analyses of the glass from ten occurrences in one of the samples from Sverrefjellet demonstrate a rather constant composition (Table 8). The compositions of the olivine and spinel which crystallized from this melt are shown in Table 9.

Table 6. Average microprobe analyses of spinel

Ref. nos.	1	2	3	4	5	6	7	8
Field nos.	GJ63.98	GJ63.97	GJ63.95	GJ62.23	GJ75.159I	GJ62.14	GJ62.21	GJ63.96
No. of anal.	1	3	3	3	12	5	3	3
TiO_2	0.32	0.10	0.29	0.08	0.07	0.08	0.05	0.07
Al_2O_3	47.93	52.43	23.49	24.53	51.69	58.21	54.76	61.45
Cr_2O_3	20.57	15.46	43.22	45.44	15.40	9.84	13.45	5.65
FeO^t	9.71	11.13	15.56	15.33	9.45	10.13	10.49	10.71
MnO	0.10	0.18	0.21	0.20	0.10	0.08	0.11	0.09
NiO	0.22	0.27	0.16	0.12	0.29	0.39	0.37	0.39
MgO	20.58	19.74	14.97	15.24	20.39	20.76	20.07	20.48
Total	99.53	99.31	97.90	100.94	97.39	99.49	99.25	98.84
Cation formulae based on 24 oxygens								
Ti	0.039	0.012	0.041	0.011	0.008	0.010	0.006	0.008
Al	9.106	9.866	5.154	5.207	9.849	10.648	10.195	11.174
Cr	2.621	1.951	6.362	6.470	1.968	1.208	1.680	0.689
Fe	1.309	1.486	2.422	2.309	1.278	1.316	1.379	1.381
Mn	0.014	0.024	0.033	0.030	0.014	0.011	0.015	0.012
Ni	0.002	0.035	0.023	0.018	0.037	0.049	0.047	0.049
Mg	4.945	4.698	4.154	4.092	4.914	4.803	4.726	4.709
Calculated:								
Fe^{2+}	1.187	1.472	2.396	2.283	1.248	1.282	1.363	1.304
Fe^{3+}	0.122	0.014	0.026	0.026	0.030	0.034	0.012	0.077
100 Mg/ $Mg+Fe^{2+}$	80.6	76.1	63.4	64.2	79.7	78.9	77.6	78.3
Cr/ $Cr+Al+Fe^{3+}$	0.22	0.17	0.55	0.55	0.17	0.10	0.14	0.06

Table 7. Average microprobe analyses of amphibole (pargasite)

Ref. no.	5
Field no.	GJ75.159I
No. of anal.	9
SiO_2	42.19
TiO_2	0.98
Al_2O_3	14.66
Cr_2O_3	1.45
FeO^t	3.07
MnO	0.07
NiO	0.12
MgO	17.55
CaO	10.21
Na_2O	3.21
K_2O	0.96
Total	94.47
Cation formulae based on 23 oxygens	
Si	6.175
Ti	0.108
Al	2.533
Cr	0.163
Fe	0.377
Mn	0.009
Ni	0.014
Mg	3.834
Ca	1.603
Na	0.912
K	0.181
Calculated:	
Fe^{2+}	0.367
Fe^{3+}	0.010
$Mg/Mg+Fe^{2+}$	0.92
$Fe^{3+}/Fe^{3+}+Al^{vi}$	0.009

Whether this intra-nodule melt has affected the surrounding olivine, spinel and clinopyroxene which it is in contact with, is questionable. The Fo content of the olivine and the Cr/(Cr + Al) ratio of the spinel are slightly higher at the melt (glass) contact than towards the interior of the crystals, which would indicate some reaction. However, these differences (Fig. 6) are within the range of olivine and spinel compositional variations of sample 6.

The presence of glass in mantle-derived peridotites has been reported in a number of cases (e.g. Frey & Green 1974, Frey & Prinz 1978, Maaløe & Printzlau 1979, MacRae 1979), and various explanations as to its origin have been proposed. Maaløe & Printzlau (1979) suggested that the partial melting occurred during contact anatexis of lherzolite surrounding a deep seated magma chamber in the mantle. Frey & Green (1974) and Frey & Prinz (1978) suggested that the heterogeneous within-nodule melts resulted from incongruent melting of hydrous phases such as phlogopite and amphibole during ascent of the host magma. MacRae (1974) stressed the absence of hydrous minerals, the apparently high mobility of the melt phase and the presence of

Table 8. Microprobe analyses of glasses in sample GJ62.14

	Glass in contact with ol, cpx and spn.					Glass in contact with ol and spn.				
SiO_2	51.99	53.78	53.05	52.89	53.17	52.50	52.18	55.21	54.58	50.53
TiO_2	2.22	1.94	2.22	2.04	2.12	1.99	2.22	1.97	1.75	2.58
Al_2O_3	20.51	20.78	20.58	21.55	21.82	20.18	20.10	20.09	20.15	21.34
Cr_2O_3	0.00	0.11	0.08	0.02	0.00	0.08	0.06	0.11	0.12	0.17
FeO^t	3.43	3.43	3.37	3.49	3.57	3.73	3.28	3.28	3.12	4.39
MnO	0.11	0.10	0.16	0.14	0.08	0.15	0.10	0.12	0.05	0.17
NiO	0.05	0.04	0.09	0.05	0.06	0.00	0.09	0.03	0.02	0.01
MgO	4.63	3.99	4.15	3.73	3.22	4.69	4.34	3.56	4.29	3.84
CaO	9.42	8.77	9.25	8.78	8.64	9.29	9.44	8.09	9.14	9.28
Na_2O	3.29	3.50	3.48	3.50	3.30	3.68	3.61	3.17	3.52	3.48
Total	95.70	96.45	96.49	96.24	96.09	96.36	95.48	95.71	96.76	95.90
$Mg/Mg+Fe^t$	0.707	0.675	0.687	0.657	0.617	0.691	0.703	0.658	0.709	0.609

Table 9. Microprobe analyses of olivine and spinel in glass from sample GJ62.14

	Olivine				Spinel	
SiO_2	40.80	41.69	41.30	40.55	–	–
TiO_2	–	–	–	–	0.50	0.75
Al_2O_3	–	–	–	–	53.15	52.46
Cr_2O_3	–	–	–	–	14.39	18.37
FeO^t	7.88	7.64	7.38	8.15	9.02	9.34
MnO	0.12	0.15	0.07	0.14	0.11	0.05
NiO	0.33	–	–	0.32	0.26	0.27
MgO	50.04	50.25	50.33	50.27	21.32	21.00
CaO	0.12	0.12	0.13	0.25	–	–
Total	99.29	99.85	99.21	99.68	98.75	102.24
Cation formulae based on 24 oxygens						
Si	5.993	6.064	6.033	9.927	–	–
Ti	–	–	–	–	0.060	0.087
Al	–	–	–	–	9.911	9.520
Cr	–	–	–	–	1.800	2.237
Fe	0.968	0.929	0.901	0.996	1.194	1.202
Mn	0.015	0.018	0.008	0.017	0.015	0.006
Ni	0.039	–	–	0.038	0.034	0.033
Mg	10.954	10.894	10.958	10.951	5.029	4.843
Ca	0.019	0.019	0.020	0.039	–	–
$100\ Mg/Mg+Fe^t$	91.9	92.1	92.4	91.7		
Calculated:						
Fe^{2+}					1.111	0.990
Fe^{3+}					0.083	0.212
$100\ Mg/Mg+Fe^{2+}$					81.9	83.0
$Cr/Cr+Al+Fe^{3+}$					0.15	0.19

vesicles in the glass, and attributed the formation of the melt to partial melting along grain boundaries influenced by CO_2-rich vapour.

The following features for the silicate glass dealt with in this account, and which may give information about its genesis, can be summarized as follows:

1. It contains vesicles, showing the presence of a gas phase.
2. Although mostly as blebs, it may also occur as a thin film along grain boundaries, indicating conditions of mobility.
3. The glass is compositionally homogeneous. There is no trace of hydrous mineral phases as

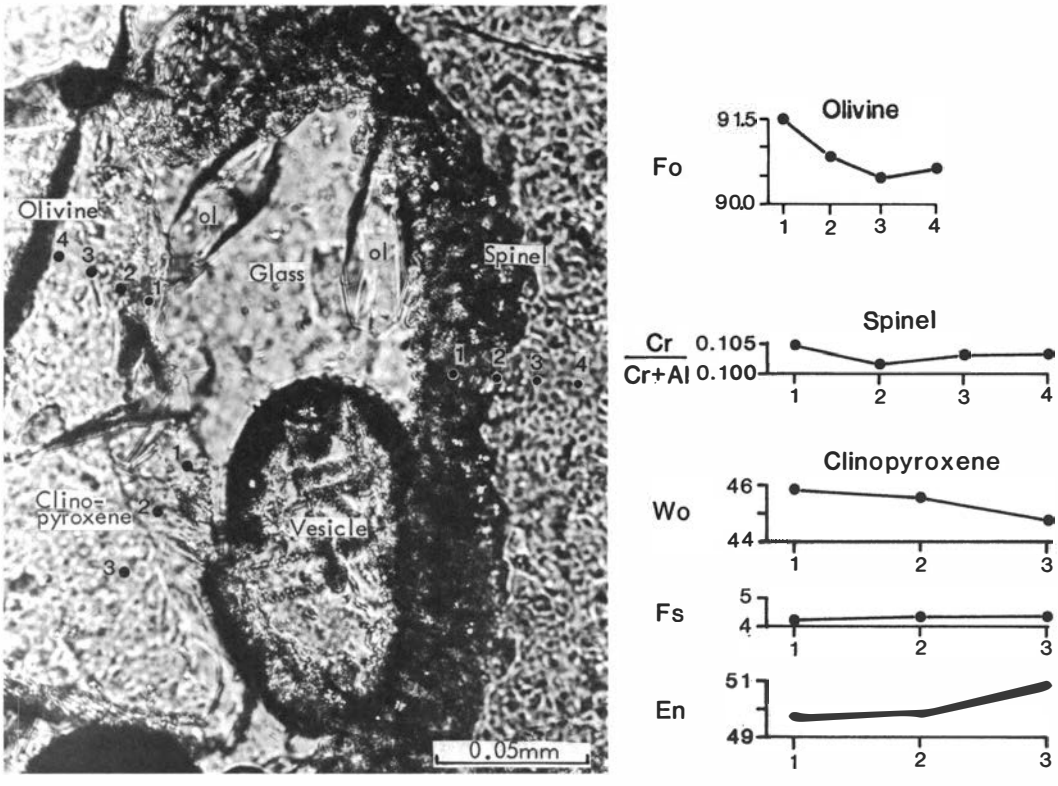

Fig. 6. Chemical profiles across olivine, clinopyroxene and spinel in contact with intra-nodule melt.

for example amphibole or mica in the glass-bearing samples, and its composition would be incompatible with melt extraction from such phases in the near complete lack of potassium. However, the high TiO_2 content of the melt is problematic. None of the observed and analysed minerals of the glass-bearing nodule (sample 6) are particularly Ti-rich. The host basalt of the nodule has a high TiO_2 content (Table 1). However, if the intra-nodule melt has been contaminated by the host basalt to yield its high TiO_2 content, the K_2O content would also have been high. This is not the case, and hence the above 'contamination model' is discarded. The only plausible explanation we can offer is that ilmenite sporadically occurred as exolution lamellae in clinopyroxene, and that melting occurred in such places. Such areas would also give the maximum number of phases, and hence be most suitable for melting.

4. There is no appreciable reaction between the melt and the surrounding host minerals. This would suggest short time between formation and quenching, probably in the order of a few hours, compared to several weeks or months residence time for the nodules in the host alkali basalt, discussed below.

In this case it therefore seems most plausible to apply the model of MacRae (1979), assuming partial melting in the presence of a gas phase (probably $CO_2 + H_2O$) during rapid ascent of the host magma.

Reaction between nodules and host basalt

Where olivine, orthopyroxene, clinopyroxene and spinel of the nodules are in contact with the host basalt, pronounced chemical variations can be seen within the outer part of the crystals. Amphibole, on the other hand, has not been observed in contact with the basalt. The analysed edge of an olivine grain adjacent to the basalt has a 0.2 mm wide zone which inwards shows a progressive compositional change from Fo 81.6 to Fo

90.4 (Fig. 7a). Orthopyroxene is separated from the basalt by a 0.1 mm to 0.2 mm thick symplectitic zone of predominantly olivine (rounded grains < 0.01 mm) with some augite. Compositionally the olivine grains within the symplectite gradually change from Fo 83.6 in contact with the basalt melt, to Fo 88.6 adjacent to the orthopyroxene (Fig. 7b). Within the orthopyroxene no significant compositional variations can be detected (Fig. 7b). Spinel shows systematic variations from the contact with the basalt melt 0.2 mm inwards (Fig. 7c). Thus Al_2O_3, MgO, NiO and Mg/(Mg + Fe^{2+}) increase continuously inwards, whereas TiO_2, FeO', MnO, Fe^{3+} and Cr/(Cr + Al + Fe^{3+}) increase outwards toward the basalt, and Cr_2O_3 is constant. Clinopyroxene in contact with basalt melt characteristically has a spongey appearance, and has, like the orthopyroxene, apparently been partially digested by the melt (Fig. 7d). In general terms there is an increase in En and decrease in Wo from the contact with the basalt inwards. The Fs content stay nearly constant around 6.5, a value which is intermediate between that of the basalt (13.4) and the average peridotite (3.8, sample 1), whereas Al_2O_3 is variable.

The above described and illustrated (Fig. 7) chemical zoning of the nodule minerals adjacent to the host basalt may be explained by two processes; 1) melting and subsequent crystallization, or 2) diffusion zoning. As to the melting-crystallization process, we find no textural evidence

Table 10. Major and trace element analyses of the spinel peridotites

Ref. nos.	1	2	3	4	5	6	7	8
Field nos.	GJ63.98	GJ63.97	GJ63.95	GJ62.23	GJ75.159I	GJ62.14	GJ62.21	GJ63.96
SiO_2	43.73	43.58	43.36	45.61	42.44	44.96	46.12	48.45
TiO_2	0.13	0.12	0.06	0.04	0.08	0.16	0.07	0.24
Al_2O_3	1.82	1.79	0.75	0.87	1.79	3.26	2.59	5.51
Cr_2O_3	0.26	0.24	0.25	0.23	0.21	0.25	0.29	0.26
Fe_2O_3	2.76	2.88	2.77	3.21	3.20	3.00	3.15	3.57
FeO	5.75	5.75	6.32	5.44	5.71	5.95	5.95	5.44
MgO	44.32	43.96	46.47	43.38	44.04	39.60	39.62	32.25
CaO	1.40	1.26	0.52	0.69	1.71	3.33	2.17	4.49
Na_2O	0.344	0.361	0.404	0.283	0.398	0.418	0.328	0.536
K_2O	0.040	0.036	0.052	0.019	0.030	0.018	0.016	0.024
MnO	0.13	0.13	0.13	0.13	0.13	0.14	0.14	0.15
P_2O_5	0.08	0.03	0.04	0.04	0.02	0.03	0.02	0.03
L.o.i.	0.12	0.19	0.53	0.12	0.64	0.35	0.29	0.59
Total	100.88	100.33	101.66	100.06	100.40	101.47	100.75	101.54
Mg/Mg+Fe	0.906	0.904	0.904	0.903	0.901	0.891	0.889	0.869
La	1.75	–	–	–	0.71	0.70	0.73	0.46
Ce	4.01	–	–	–	1.82	–	–	–
Nd	–	–	–	–	1.05	–	1.32	1.89
Sm	0.66	–	–	–	–	–	–	–
Eu	0.16	–	–	–	0.12	0.04	0.14	0.21
Gd	0.56	–	–	–	0.37	–	0.38	–
Tb	0.05	–	–	–	0.05	0.02	0.06	0.14
Ho	0.06	–	–	–	0.07	0.04	0.11	0.24
Tm	0.03	–	–	–	0.03	0.02	0.05	0.10
Yb	0.17	–	–	–	–	0.12	0.34	0.61
Lu	–	–	–	–	0.03	0.02	–	0.12
Cs	0.04	–	–	–	0.03	0.08	0.03	0.06
Hf	0.47	–	–	–	0.27	0.22	0.52	0.44
Ta	0.03	–	–	–	0.02	0.004	0.002	0.008
Th	0.38	–	–	–	0.20	0.18	0.16	0.10
U	0.78	–	–	–	0.73	0.61	0.89	0.55
Sc	7.86	–	–	–	8.41	8.50	13.20	16.17
V	29	28	13	17	26	50	41	87
Cr	2287	2046	2201	2032	1839	2199	2507	2248
Co	105	–	–	–	108	78	101	80
Ni	2048	2092	2271	2078	2076	1886	1937	1424
Zn	48	50	52	45	43	52	50	56

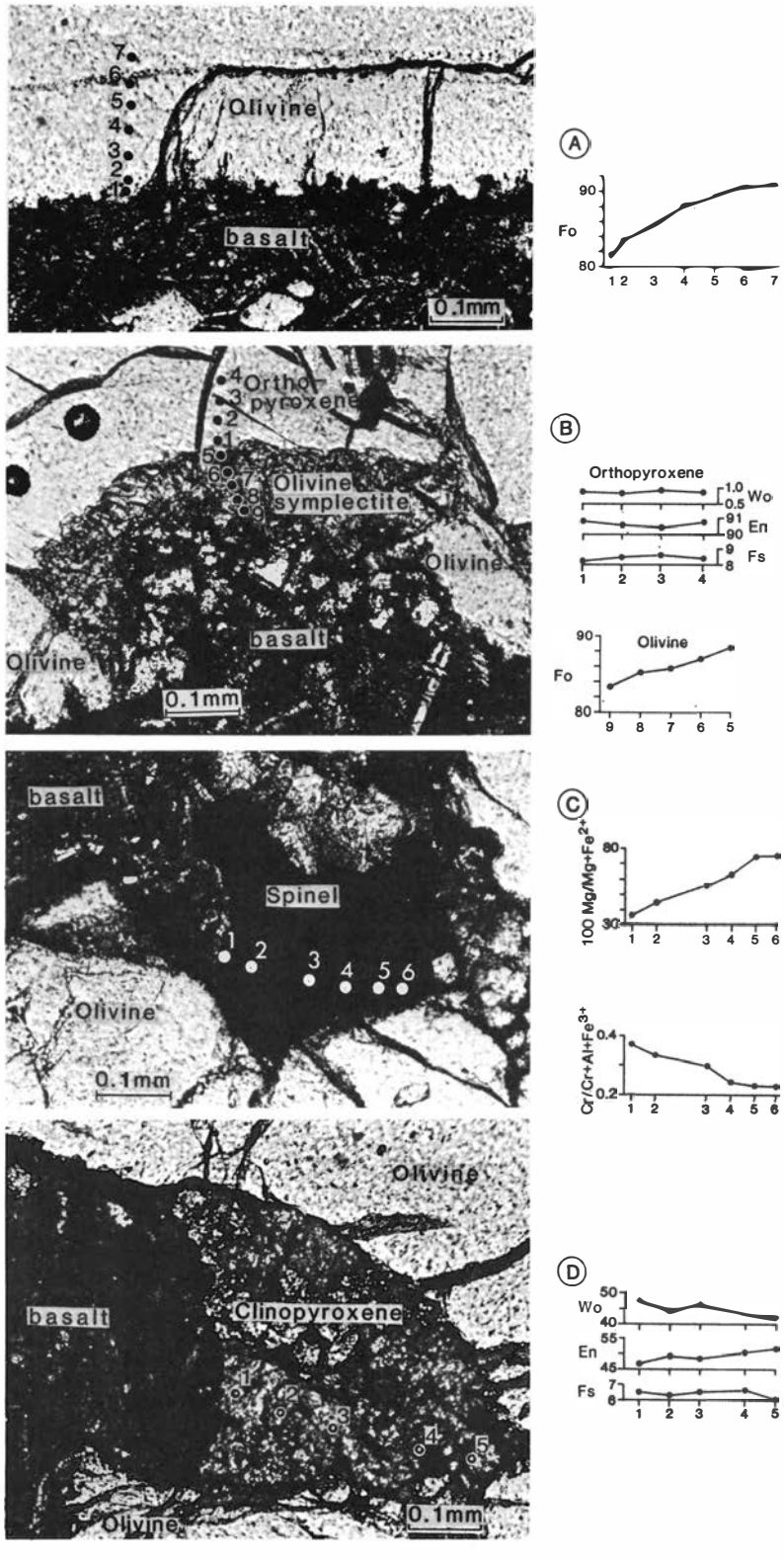

Fig. 7. Chemical variations across mineral edges adjacent to the host basalt.
A: Olivine-basalt melt,
B: Orthopyroxene-basalt melt,
C: Spinel-basalt melt,
D: Clinopyroxene-basalt melt.

Table 11. Partition coefficients used in petrogenetic modelling

	Ol	Opx	Cpx	Spn
La	0.0005	0.0005	0.2	0.03
Nd	0.0013	0.0019	0.09	0.035
Eu	0.0019	0.0036	0.16	0.055
Tb	0.0019	0.0059	0.19	0.08
Yb	0.0040	0.0286	0.20	0.1

Partition coefficients for olivine, orthopyroxene and clinopyroxene: from Frey et al. (1978). For spinel: from Irving (1978).

in the olivine and spinel grains for such a process, and for which the gradual chemical changes in the olivine and spinel, as demonstrated in Fig. 7, probably would also argue against. By regarding the diffusion zoning as a more probable process it is possible to give some estimates on the residence time of nodules in the host basalt prior to extrusion, given by the equation $t > x^2/D$, where x is the thickness of the chemically zoned margin and D is the diffusion coefficient (Halloran and Bowen 1980). The thickness of the reaction zone in olivine and spinel is about 200 μ (Fig. 7). By using the diffusion coefficient of Mg^{2+} in olivine ($D_{Mg^{2+}} = 7.6 \times 10^{-11}$ cm^2 s^{-1}) (Hermeling & Schmalzried 1984) atT = 1130°C, the residence time of this nodule (sample 1) in the basalt is about 61 days. The diffusion coefficients of Fe^{2+} in spinel are 10^{-9} cm^2 s^{-1} at T = 1400°C and 10^{-11} cm^2 s^1 at = 1100°C (Halloran & Bowen 1980). If we assume a linear relationship between temperature and diffusion coefficients, i.e. $D_{Fe^{2+}} \sim$ ca. 2×10^{-11} for spinel at T = 1130°C (equal to that calculated for olivine), the calculated residence time is about 230 days. By choosing T = 1200°C, however, the residence time (for spinel) is about 66 days. Even though these conservative time estimates show somewhat variable results they nevertheless indicate the order of magnitude for residence time of the nodules in the magma. It should also be pointed out that the analysed minerals may have become in contact with the basalt melt at different time as the liquid penetrated and broke up the nodules.

Bulk rock geochemistry

Major oxide compositions. – The bulk rock geochemistry of the spinel peridotites is shown in Table 10. There is a general relationship between MgO/(FeO + 0.9 Fe_2O_3) (or Mg/(Mg + Fe)) ratios and oxide contents. As the above-mentioned ratios increase, SiO_2, Al_2O_3, TiO_2 and CaO decrease, whereas MgO increases (Fig. 8). Such relationships have been described from a number of lherzolite nodules elsewhere (Kuno & Aoki 1970, Harris et al. 1972, Maaløe & Aoki 1977, Frey & Green 1974, Hutchinson et al. 1975, Rodgers et al. 1975, Frey & Prinz 1978), and it is believed that those with the lowest and highest

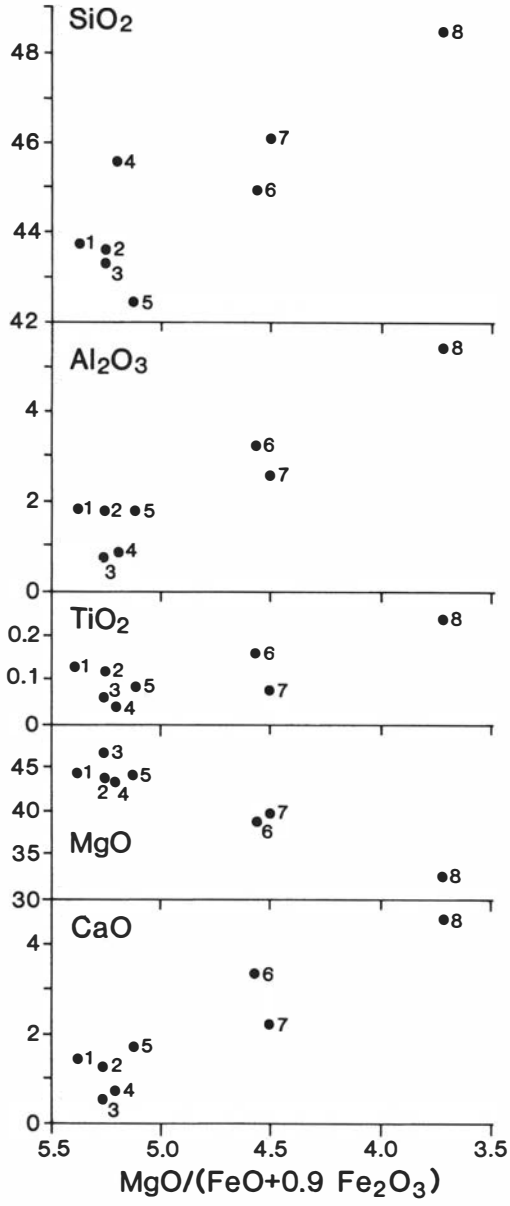

Fig. 8. Relationships between bulk rock oxides and MgO/(FeO + 0.9 Fe_2O_3).

Mg/(Mg + Fe) ratios represent the most primary, and the most depleted residual mantle, respectively, although as pointed out by Frey & Prinz (1978), this feature may not be generally conclusive. However, if these rocks represent cumulates, larger ranges than those observed for the compatible elements Cr, Co and Ni (Table 10), as discussed by Frey & Prinz (1978), would be expected, and the spinel-peridotite nodules are thought to represent mantle samples. The small range in Fo (88–92, Table 3) may also suggest the same.

Trace element abundances. – Table 10 shows the trace element abundance of the spinel peridotites. Their chondrite-normalized REE patterns are shown in Fig. 9. Samples 1, 5 and 6 are characterized by depletion in HREE to MREE (Lu: 0.7–0.9 times chondrite), and enrichment in LREE (La: 2.2 to 5.1 times chondrite). Sample 7 shows a slight increase in the chondrite-normalized values from Yb to La (ca. 1.9 to 2.2 times chondrite), whereas sample 8 shows a flat pattern from Lu through Nd (ca. 3 times chondrite), and depletion in La (ca. 1.4 times chondrite). These concentration levels and patterns are rather similar to those of dunites, harzburgites and lherzolites from San Carlos, Arizona, described by Frey & Prinz (1978). The elements Ta and Th and to some extent U show the same trend as La, i.e. lowest concentrations in sample 8. The abundances of the transition metals Sc, Co and Ni, whose solid/liquid partition coefficients are normally greater than unity, correlate with the modal compositions of the nodules. Thus Sc increases as modal clinopyroxene increases, whereas Co and Ni increase as modal olivine increases. The behaviour of Cr is more complex since it is partitioned into both pyroxenes and strongly (but variably) into spinel (Tables 4, 5 and 6).

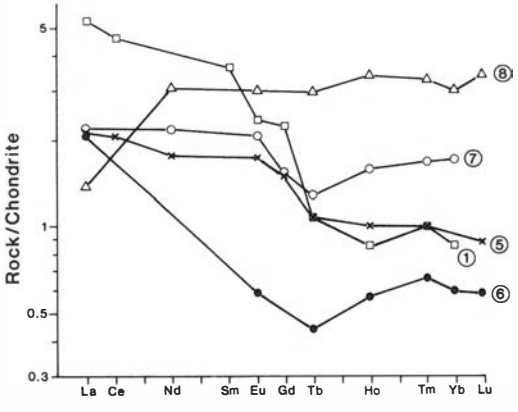

Fig. 9. Chondrite-normalized REE paterns of the spinel peridotites. Chondrite-data from Haskin et al. (1968).

Petrogenetic considerations

The spinel peridotites

In general there is a good relationship between the mineral composition of the spinel lherzolites and their major and compatible trace element compositions. The most clinopyroxene-rich samples are those which have the highest contents of CaO, Al_2O_3, SiO_2, Sc and V, whereas the olivine-rich samples have the highest MgO, Ni and Co values. Chromium, however, which is also a strongly compatible element, does not show any good relationship with the modal composition. These relationships would be compatible with increasingly higher degrees (or increasing numbers of episodes) of partial melting to progressively deplete the residue in clinopyroxene and spinel and hence Al, Ca and Sc, and cause a progressive modal enrichment in the highly refractory olivine (and Ni and Co). From the relationships between Al_2O_3 and CaO in the bulk rock and the forsterite contents of olivine, it is proposed that at least two different source materials (group 1 composed of samples 1, 5, 6, 7 and 8, and group 2 composed of samples 2, 3 and 4) existed prior to this or these earlier proposed partial melting event(s).

However, the highly incompatible elements such as LREE, Cs, Ta, Th, U and K do not follow the expected trend for the above-mentioned model, and suggest a more complicated evolution. Indeed, the most refractory sample of group 1 (sample 1), has the highest content of La, Th, U and K, whereas sample 8 (the least refractory) has the lowest content of these elements (Table 10).

Similar patterns have been observed in mantle-derived spinel- and garnet lherzolites, and a model has been proposed whereby depleted and refractory mantle gets enriched in the highly incompatible elements by getting veined or metasomatized by liquids produced by small (< 1%) degrees of partial melting of garnet lherzolite (Frey & Green 1974, Frey & Prinz 1978, Ehrenberg 1982, Wilshire 1984). Such a model would probably explain the relationships between the modal compositions, major oxides, compatible

and incompatible trace element abundances of the spinel peridotite nodules dealt with in this account.

The enrichment of incompatible elements in the refractory mantle peridotite would have to be produced by the introduction of liquids strongly enriched in LREE and strongly depleted in HREE, since apparently *only* the LREE and Th, U and K have been enriched in the refractory samples (Fig. 9). Even though a small degree of partial melting of a garnet peridotite (in which garnet is a residual mineral after melting) would easily yield a liquid with the above-required REE pattern, partial melting from a spinel peridotite would also satisfy the same requirements depending on its REE pattern (LREE enriched, HREE depleted).

The host basalt

The high MgO and Ni contents of the basalt would indicate that only a limited amount of crystal fractionation had occurred from the primary basalt liquid. Since plagioclase and clinopyroxene occur only as quench crystals, it is most likely that only olivine, which occurs as small phenocrysts, could have been a fractionating mineral. By accounting for 15% olivine fractionation, this would yield a basalt with about 15% MgO, a value which would be well within the range, and probably near to that of a primary basalt (Maaløe 1979, Maaløe & Jacobsen 1979, Elthon 1979). Olivine fractionation of this order would, however, result in only a minor increase in the incompatible trace element abundances, and the REE pattern of such a 'primary' basalt is shown in Fig. 10.

The shape of the REE pattern of the host basalt is rather unusual in its pronounced change from a steep pattern between La and Tb, and a flat pattern between Tb and Lu (Fig. 10). Alkaline basalts are generally believed to be produced by small degrees of partial melting of garnet-bearing lherzolites, and their REE patterns are consistently steep between La and Lu (e.g. Kay & Gast 1973). The REE pattern of the host basalt discussed here is difficult to reconcile with those expected in basalts generated from, and in equilibrium with, garnet-peridotites.

Below we discuss the possibility that the host basalt represents a partial melt derived from a spinel peridotite source of which the analysed nodules are representative. Judging from their different REE paterns (Fig. 9) and mineral compositions (Table 2), undoubtedly the source must be heterogenous with respect to incompatible trace elements as well as modal composition, and probably even more varied than is indicated by the five samples presented here. In order to reproduce approximately the steep REE pattern between La and Tb of the host basalt, only small degrees (in the order of 1–3%) of partial melting of the nodule material are permitted. As the most realistic model, we have therefore chosen batch melting (Hanson 1978), where the produced liquid will be in chemical equilibrium with the remaining solid at the time of melt migration, since the residual mantle after a small percentage of partial melting will have approximately the same modal proportions as prior to melting. Hence, even if the liquid should be removed from its source before complete equilibration has occurred, this will have little effect on the liquid.

The REE pattern of the mantle source has been modelled using the modal compositions of the nodules and the REE abundance of the host basalt as known parameters. The patterns calculated for 1, 3 and 5% partial melting have characteristics and total abundances somewhat similar

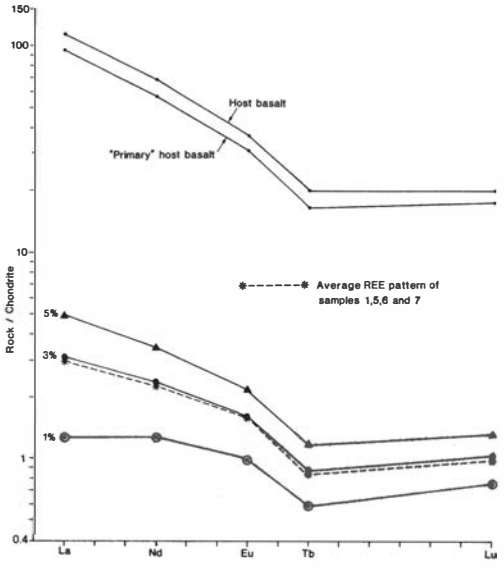

Fig. 10. The upper part of the illustration shows the REE patterns of the host basalt, and its estimated 'primary' composition. The lower part shows the calculated REE patterns of the modal mantle (average modal composition of samples 1, 5, 6, 7 and 8), which would yield the REE pattern of the 'Primary' host basalt by 1, 3 and 5% equilibrium melting. The average REE pattern of samples 1, 5, 6 and 7 is shown, and it fits very closely with the modal implying 3% partial melting from the modal mantle.

to the average REE pattern of the nodules. A perfect fit is, however, obtained by 3% partial melting when the LREE depleted pattern of sample 8 is subtracted from the average REE pattern of the nodules (Fig. 10).

It may therefore be concluded that the REE pattern of the host basalt can be produced by 3% partial melting of a mantle source that has an average REE pattern similar to the average of the LREE enriched nodules and a modal composition similar to the average of the REE analysed samples (1, 5, 6, 7 and 8), i.e. $Ol_{0.58}$ $Opx_{0.28}$ $Cpx_{0.12}$ $Sp_{0.02}$.

Conclusions

The main features of the Al-spinel and Cr-spinel peridotite nodules and their host basalt from the Quaternary volcanos (mainly the Sverrefjellet volcano) in Vestspitsbergen can be summarized as follows:

1. Their modal composition ranges from harzburgite, lherzolite to olivine websterite. Lherzolite is the most common type.
2. Texturally most of them can be classified as the protogranular type with culvilinear grain boundaries. Little evidence of exolution is preserved, and when present, it is confined to the central area of host crystals.
3. In terms of mineral chemistry, olivine ranges between Fo 88.1 to 92.0. Orthopyroxene shows a range in the 100 Mg/(Mg + Fe^t) ratio between 88.9 and 92.3, and the most pronounced variations are in the Al_2O_3 and Cr_2O_3 contents. Clinopyroxene is a chrome diopside with the largest variations in Al_2O_3 and TiO_2. The spinel (Al-spinel and Cr-spinel) show large variations in FeO^t, Al_2O_3 and Cr_2O_3, particularly the latter (5.65–45.44 wt.%). Amphibole, recorded in one sample, is a pargasite.
4. The major oxide and compatible element abundances correspond with the modal composition, i.e. those richest in clinopyroxene contain most CaO, Al_2O_3 and Sc, whereas the olivine-richest samples have the highest MgO, Ni and Co values.
5. The highly incompatible elements such as La, Ta, Th, U and K are lower in the olivine websterite and lherzolite than the more refractory nodules which straddle the lherzolite/harzburgite boundary. The REE patterns of the nodules show a variety of shapes.
6. The host basalt has an unusual REE pattern with a steep slope between La and Tb, and a flat pattern between Tb and Lu.
7. Reaction between the host basalt and the nodule minerals would indicate a nodule residence time in the magma of about 2 months. Intra-nodule melt, however, shows little if any reaction with the nodule minerals, and was probably produced during the rapid ascent of the basalt.

A plausible explanation for these features would be that prior to the Quaternary volcanism, the mantle beneath Spitsbergen had suffered basalt extraction leaving behind variously depleted residues. These residues were subsequently enriched in highly incompatible elements, probably by the veining or metasomatic effects of a partial melt generated from garnet lherzolite. The Quaternary basalt can be modelled (on the basic of REE pattern) by 3% equilibrium melting of this heterogeneous source of spinel peridotites whose average modal composition would be $Ol_{0.58}$ $Opx_{0.28}$ $Cpx_{0.12}$ $Sp_{0.02}$.

Acknowledgements. – Dr. T. Gjelsvik provided us with the material for this study. Dr. J. Boyle and two anonymous reviewers gave constructive comments to the manuscript, and E. Irgens and J. Ellingsen prepared the illustrations. We thank all these persons.

References

Anders, O. H. 1969: Experiences with the Ge (Li)-detector of high-resolution gamma ray spectrometry and a practical approach to the pulse pileup problem. *Nud. Instr. methods 6,* 205.

Baedecker, P. A., Rowe, J. & Steinnes, E. 1977: Application of epithermal neutron activation in multielement analysis of silicate rocks employing both coaxial Ge (Li) and low energy photon detector system. *J. Radioanal. Chem. 40,* 115–146.

Brown, G. M., Pinsent, R. H. & Coisy, P. 1980: The petrology of spinel-peridotite xenoliths from the Massif Central, France. *Am. J. Sci. 280-A,* 471–498.

Brunfelt, A. O. & Steinnes, E. 1969: Instrumental activation analyses of silicate rocks with epithermal neutrons. *Anal. Chim. Acta. 48,* 13–24.

Brunfelt, A. O. & Steinnes, E. 1971: A neutron activation scheme developed for the determination of 42 elements in Lunar material. *Talanta 18,* 1197–1208.

Carswell, D. A. 1980: Mantle derived lherzolite nodules associated with kimberlite, carbonatite and basalt magmatism: A review. *Lithos 13,* 121–138.

Colby, J. B. 1968: MAGIC IV – a computer program for quantitative electron microprobe analysis. *Adv. X-Ray Anal. 11,* 287–306.

Covell, D. F. 1959: Determination of gamma abundances directly from the total absorption peak. *Anal. Chem. 31,* 1783.

Delaney, J. S., Smith, J. V. & Nixon, P. H. 1979: Model for upper mantle below Malaita, Solomon Islands, deduced from chemistry of lherzolite and megacryst minerals. *Contrib. Mineral. Petrol. 70,* 209–218.

Ehrenberg, S. N. 1982: Rare earth element geochemistry of garnet lherzolite and megacrystalline nodules from minette of the Colorado Plateau province. *Earth. Planet. Sci. Lett. 57,* 191–210.

Elthon, D. 1979: High magnesia liquids as the parental magma for ocean floor basalt. *Nature 278,* 514–518.

Flanagan, F. J. 1973: 1972-values for international reference standards. *Geochim. Cosmochim. Acta 37,* 1189–1200.

Flanagan, F. J. 1976: Description and analyses of eight new USGS rock standards. *Geol. Surv. Prof. Pap. 840,* 192 pp.

Foss Amundsen, H. E. 1984: Structure of the lower crust/upper mantle under NW-Spitsbergen, basen on Quarternary Xenolith-material. (Abstract). *Norsk Geologisk Forening, Geologgnytt Nr. 20,* 23.

Frey, F. A. & Green, D. H. 1974: The mineralogy, geochemistry and origin of lherzolite inclusions in Victoria basanites. *Geochim. Cosmochim. Acta 38,* 1023–1059.

Frey, F. A. & Prinz, M. 1978: Ultramafic inclusions from San Carlos, Arizona; Petrologic and geochemical data bearing on their petrogenesis. *Earth. Planet. Sci. Lett. 38,* 129–176.

Frey, F. A., Green, D. H. & Roy, S. D. 1978: Integrated models of basalt petrogenesis: A study of quartz tholeiites to olivine melilitites from South Eastern Australia utilizing geochemical and experimental petrological data. *J. Petrol. 19,* 463–513.

Gjelsvik, T. 1963: Remarks on the structure and composition of the Sverrefjellet volcano, Bockfjorden, Vestspitsbergen. *Norsk Polarinst. Årbok 1962,* 50–54.

Griffin, W. L., Wass, S. Y. & Hollis, J. D. 1984: Ultramafic xenoliths from Bullenmerri and Gnotuk Maars, Victoria, Australia: Petrology of a subcontinental crust-mantle transition. *J. Petrol. 25,* 53–87.

Halloran, J. W. & Bowen, H. K. 1980: Iron diffusion in iron-aluminate spinels. *J. Am. Ceram. Soc. 63,* 58–65.

Hanson, G. N. 1978: The application of trace elements to the petrogenesis of igneous rocks of granitic composition. *Earth. Planet. Sci. Lett. 38,* 26–43.

Harris, P. G., Hutchinson, R. & Paul, D. K. 1972: Plutonic xenoliths and their relation to the upper mantle. *Philos. Trans. R. Soc. London. Ser. A 271,* 313–323.

Haskin, L. A., Haskin, M. A., Frey, F. A. & Wildeman, T. R. 1968: Relative and absolute terrestrial abundances of the rare earths. In: Ahrens LH (ed). *Origin and Distribution of the Elements.* Pergamon Press, New York, pp. 889–912.

Hermeling, J. & Schmalzried, H. 1984: Tracerdiffusion of the Fe-cations in olivine Fe_xMg_{1}-x)$_2$ SiO_2 (III). *Phys. Chem. Minerals 11,* 161–166.

Hoel, A. 1914: Nouvelle observations sur le district volcanique du Spitsberg du nord. *Vid. Selsk. Skr. 1. Mat. Nat. Kl. No. 9. Kristiania,* 33 pp.

Hutchinson, R., Chambers, A. L., Paul, D. K. & Harris, P. G. 1975: Chemical variation among French ultramafic xenoliths – evidence for a heterogeneous upper-mantle. *Mineral. Mag. 40,* 153–170.

Irving, A. J. 1978: A review of experimental studies of crystal/liquid trace element partitioning. *Geochim. Cosmochim. Acta 42,* 743–770.

Kay, R. & Gast, P. W. 1973: The rare earth content and origin of alkali-rich basalts. *J. Geol 81,* 653–682.

Kuno, H. & Aoki, K. 1970: Chemistry of ultramafic nodules and their bearing on the origin of basaltic magma. *Phys. Earth. Planet. Interiors 3,* 273–301.

Kurat, G., Palme, H., Spettel, B., Baddenhausen, H., Hofmeister, H., Palme, C. & Wänke, H. 1980: Geochemistry of ultramafic xenoliths from Kapfenstein, Austria: evidence for a variety of upper mantle processes. *Geochim. Cosmochim. Acta. 44,* 45–60.

Kyser, T. K., & O'Neil, J. R., & Carmichael, I. S. E. 1982: Genetic relations among basic lavas and ultramafic nodules: evidence from oxygen isotope compositions. *Contrib. Mineral. Petrol. 81,* 88–102.

Maalø, S. 1979: Compositional range for primary tholeiitic magmas evaluated from major-element trends. *Lithos 12,* 59–72.

Maaløe, S. & Aoki, K. 1977: The major element composition of the upper mantle estimated from the composition of lherzolites. *Contrib. Mineral. Petrol. 63,* 161–173.

Maaløe, S., & Jakobsson, S. P. 1979: The PT phase relations of a primary oceanite from the Reykjanes peninsula, Icland. *Lithos 13,* 237–246.

Maaløe, S. & Printzlau, I. 1979: Natural partial melting of spinel lherzolite. *J. Petrol. 29,* 727–741.

MacRae, N. D. 1979: Silicate glass and sulfides in ultramafic xenoliths, Newer Basalts, Victoria, Australia. *Contrib. Mineral. Petrol. 68,* 275–280.

Mercier, J. C. C., & Nicolas, A. 1975: Textures and fabrics of upper-mantle peridotites as illustrated by xenoliths from basalts. *J. Petrol. 16,* 454-487.

Padfield, T., & Gray, A. 1971: Major element rock analyses by X-ray fluorescence – a simple fusion method. NV Phillips, analytical equipment FS 35, Eindhoven.

Prestvik, T. 1978: Cenozoic plateau lavas of Spitsbergen – a geochemical study. *Norsk Polarinst. Årbok 1977,* 129–143.

Reed, S. J. B. 1975: *Electron Microprobe Analyses.* Cambridge University Press, London, 400 pp.

Rodgers, K. A., Brothers, R. N. & Searle, E. J. 1975: Ultramafic nodules and their host rocks from Auckland, New Zealand. *Geol. Mag. 112,* 163–174.

Sterlinski, S. 1968: Analyses of digital data from a multichannel pulse height analysic on gamma ray total absorption peaks in activation analyses. *Anal. Chem. 40,* 1995.

Wilshire, H. G. 1984: Mantle metasomatism: The REE story. *Geology 12,* 395–398.